Article ID 1004-924X(2004)03-0292-05

H-MRTD simulation of dual-frequency miniature patch antenna

YU Wen-ge[1,2], ZHONG Xian-xin[1], LI Xiao-yi[1], CHEN Shuai[1]

(1. *The Key Lab for Optoelectronic Technology & Systems of Ministry of Education, Chongqing University, Chongqing* 400044, *China;*
2. *Basic Logistical Engineering University, Chongqing* 400016, *China*)

Abstract: A novel MEMS dual-band patch antenna is designed using slot-loaded and short-circuited size-reduction techniques. By controlling the short-plane width, f_{10} and f_{30}, two resonant frequencies, can be significantly reduced and the frequency radio (f_{30}/f_{10}) is tunable in the range 1.7~2.3. The Haar-Wavelet-Based multiresolution time domain (H-MRTD) is used for modeling and analyzing the antenna for the first time. In addition, the mathematical formulae are extended to an inhomogenous media. Numerical simulation results are compared to those achieved using the conventional 3-D finite-difference time-domain (FDTD) method and measured. It has been demonstrated that, with this technique, space discretization with only a few cells per wavelength gives accurate results, leading to a reduction of both memory requirements and computation time.

Key words: dual-frequency antenna; H-MRTD method; FDTD method; MEMS; UPML absorbing boundary conditions

双频微型贴片天线的 H-MRTD 模拟

余文革[1,2], 钟先信[1], 李小毅[1], 陈 帅[1]

(1. 重庆大学 光电技术及系统教育部重点实验室, 重庆 400044; 2. 后勤工程学院基础部, 重庆 400016)

摘要: 利用槽隙加载及短接技术设计了双频小型微带天线。通过调节短接面宽度, 两谐振频率f_{10}及f_{30}可明显降低, 天线尺寸显著减小, 而且频比(f_{30}/f_{10})的可调范围为 1.7~2.3。首次将三维 H-MRTD (Haar-Wavelet-Based Multiresolution Time Domain)全波分析方法应用于该天线的建模和分析, 并将 H-MRTD 数值计算公式推广到了非均匀有耗媒质中。数值模拟结果同传统 FDTD(Finite Difference Time Domain)方法及实验结果进行了比较。结果表明, 每个波长只需取较少的空间离散网格, 三维 H-MRTD 时域全波分析方法便能较精确地模拟微机械微带天线, 并能有效地减少 CPU 计算时间及节省计算机内存。

关 键 词: 双频天线; H-MRTD 方法; FDTD 方法; 微机械; UPML 吸收边界条件
中图分类号: TN823 文献标识码: A

1 Introduction[1]

Recently, patch antenna research has focused on reducing the size of the patch, which is important in many commercial and military applications. It has been shown that the resonant frequency of a microstrip antenna can be significantly reduced by introducing a short-circuited plane or a partly short-circuited plane

Received date: 2003-11-27; **Revised**: 2004-02-16.

Foundation item: Project Supported by the Major State Basic Research Development Program, "Integrated Micro-Optical-Electronic Mechanical System" (Project No. G1999033105).

where the electric field of the resonant mode is zero[1-3], or a short-pin near the feed probe[4]. Using two stacked short-circuited patches, dual-frequency operation has been obtained[5]. However, the use of a stacked geometry leads to increases in the thickness and complexity of the patch. In this paper, we demonstrate that by short-circuiting the zero potential plane of a slotted patch excited with a dominant mode (TM_{10}), the resonant frequencies, f_{10} and f_{30}, of the two operating modes can be approximately halved and can even be significantly reduced by decreasing the shorted-plane width. This indicates that a large reduction in antenna size can be obtained by using the proposed design, as compared to that of a regular slot-loaded patch.

The finite-difference time-domain (FDTD) method[6] is widely used for solving problems related to electromagnetism. However, there still exist many restrictive factors, such as memory shortage and CPU time, etc. we first adopted the method of the Haar-Wavelet-Based Multiresolution Time Domain (H-MRTD)[7-9] with compactly supported scaling function for a full three-dimensional (3-D) wave to Yee's staggered cell to analyze and simulate the dual frequency microstrip antenna. The major advantage of the MRTD algorithms is their capability to develop real-time time and space adaptive grids through the efficient thresholding of the wavelet coefficients. Using this technique, space discretization with only a few cells per wavelength gives accurate results, leading to a reduction of both memory requirement and computation time. Associated with practical model, a uniaxial perfectly matched layer (UPML) absorbing boundary conditions[10] was developed, a three-dimensional formulation of the discrete difference equations arising from the Maxwell's system is first extended to an inhomogenous medium, it is applied to the analysis of dual-frequency miniature patch antenna.

2　Dual-frequency slot-loaded patch antenna

2.1　Design of slot-loaded patch antenna

The layout of the slot-loaded patch antenna designed in this paper is shown in Fig. 1. A single slot with dimensions $L \times W$ is cut in a rectangular patch with dimensions $a \times b$ with a short-circuited plane of width placed at its other side. The parameters of the antenna are a= 38 mm, b= 25 mm, L= 36 mm, W= 1 mm, d= 2 mm, h= 3 mm, r= 1 mm, respectively. Owing to being compatible with standard IC technology, and prone to integration with other components, silicon wafer (ε_r= 11.7) was selected as a layer of microstrip substrate. Between the ground plate and the wafer there is a layer of foam (ε_r = 1.07), which could suppress surface wave induced in the wafer substrate, as a result, the efficiency and the bandwidth of the antenna were increased, and the radiation pattern improved.

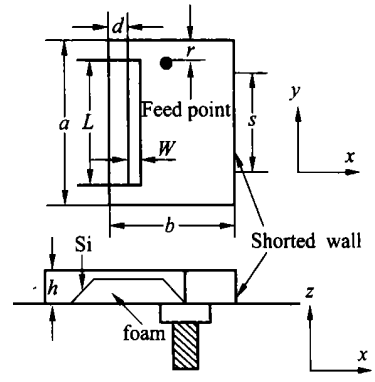

Fig. 1　Geometry of dual-band slot-loaded microstrip antenna

2.2　Measured results

The parameters of the slot antenna are selected as above mentioned. The measurements carried out on an Agilent 8720C vector network analyzer. It is then found that, by controlling the shorted-plane width, both the TM_{10} and TM_{30} modes are strongly perturbed. Fig. 2 shows typical results of the measured return loss for the cases with s/a= 1, 0.25, and 0.1. Regarding the

results shown in Fig. 2, it can be seen that the perturbed TM_{10} and TM_{30} modes are excited with good impedance matching. However, when $s/a < 0.1$, there no feed point can be found for exciting the two frequencies with good impedance matching. This indicates that there are limitations to the present dual-band design. It can be seen that the obtained frequency ratio (f_{30}/f_{10}) of the two frequencies for present design varies in the range 1.7~ 2.3. On the other hand, for the case $s/a = 0.1$, shown in Fig. 2, the frequency f_{10} occurring at 1.562 GHz is ~ 0.31 times that (5.038 GHz) for a regular half-wavelength patch with the same patch size. In other words, the size of the designed antenna in this paper is much smaller than regular half-wavelength patch antenna.

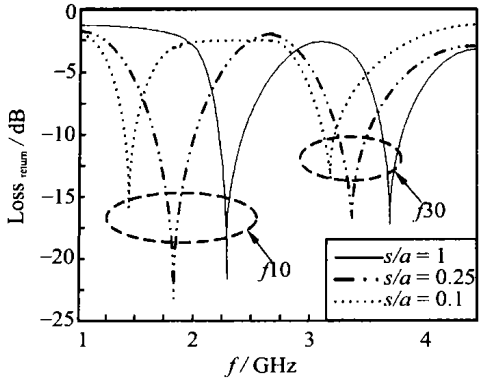

Fig. 2 Measured return loss for different shorted-plane widths

3 3-D H-MRTD algorithm

3.1 Numerical formulations of the 3-D H-MRTD method

Maxwell's curl equations in an isotropic medium:

$$\begin{cases} \nabla \times \boldsymbol{E} = -\mu \dfrac{\partial \boldsymbol{H}}{\partial t} \\ \nabla \times \boldsymbol{H} = \varepsilon \dfrac{\partial \boldsymbol{E}}{\partial t} + \sigma \boldsymbol{E}, \end{cases} \tag{1}$$

where ε is permittivity, μ is permeability, σ is electric conductivity. Each field component is expanded into scaling functions:

$$\varphi_u(s) = \varphi(s/\Delta s - u), \tag{2}$$

and wavelets:

$$\psi_u(s) = \psi(s/\Delta s - u), \tag{3}$$

where, $\begin{cases} \varphi(s) = 1, \ s \in (0, 1) \\ \varphi(s) = 0, \text{otherelse.} \end{cases}$

and $\psi(s) = \varphi(2s) - \varphi(2s-1)$.

Expansion and testing is performed for each spatial coordinate $s = \{x, y, z\}$ with corresponding discretization indices $u = \{k, l, m\}$, as well as for time with rectangular pulse $h_n(t)$. In compact notations, the x-directed electric field component in the staggered Yee's grid of size Δx, Δy, Δz is represented as

$$E_x(x, y, z, t) = \sum_{klm} \sum_{\xi\eta\zeta} \sum_n {}^{\xi\eta\zeta}_{k+1/2,\,l,\,m}E^n \cdot \xi_{k+1/2}(x)\,\eta_l(y)\,\zeta_m(z)\,h_n(t), \tag{4}$$

where $x = k\Delta x$, $y = l\Delta y$, $z = m\Delta z$, $t = n\Delta t$.

The summation over $\xi\eta\zeta$ includes eight terms stemming from all the permutations of scaling functions and wavelets:

$$\xi\eta\zeta = \{\varphi\varphi\varphi,\ \varphi\varphi\psi,\ \varphi\psi\varphi,\ \varphi\psi\psi,\ \psi\varphi\varphi,\ \psi\varphi\psi,\ \psi\psi\varphi,\ \psi\psi\psi\}$$

The representation of the other field components is easily derived through permutation of the indices and follows the same rule as for standard FDTD scheme. Inserting the above expressions into the difference equations and performing a Galerkin test procedure[12] leads to the following expressions for the electric field within each cell $\{k, l, m\}$:

$${}^{x}_{3}E^{\xi\eta\zeta}_{100} - {}^{x}_{0}E^{\xi\eta\zeta}_{100} = \frac{\Delta t}{\varepsilon} \cdot \left\{ \frac{{}^{z}_{1}H^{\xi\eta\zeta}_{110} - {}^{z}_{1}H^{\xi\eta\zeta}_{120}}{\Delta y} - \frac{{}^{y}_{1}H^{\xi\eta\zeta}_{101} - {}^{y}_{1}H^{\xi\eta\zeta}_{102}}{\Delta z} - \sigma \cdot {}^{x}_{1}E^{\xi\eta\zeta}_{100} \right\}. \tag{5}$$

where $\{0, 1, 2, 3\}$ denotes, respectively, $\{u, u+1/2, u-1/2, u+1\}$ for each $u = \{k, l, m, n\}$. In formula (5), there are three different E_x values within one time step, this brings about inconvenience for program design. In order to avoid the shortcoming, we can adopt approximation as follows:

$${}^{x}_{1}E^{\xi\eta\zeta}_{100} = \frac{1}{2}\left({}^{x}_{3}E^{\xi\eta\zeta}_{100} + {}^{x}_{1}E^{\xi\eta\zeta}_{100} \right), \tag{6}$$

Similar expressions are obtained for the other field components.

3.2 Absorbing boundary condition

The field computation domain must be limited in size because the computer can not store an unlimited amount of data. The computation domain must be large enough to enclose the structure of interest. In this paper, we adopted uniaxial perfectly matched layer (UPML) absorbing boundary conditions. Consider one dimension wave equation propagated along + z direction:

$$\left(\frac{\partial}{\partial z}-\frac{1}{v}\frac{\partial}{\partial t}\right)E_x-\frac{\sigma'}{v}E_x=0, \tag{7}$$

where $\sigma'=\sigma/\varepsilon$, v is the phase velocity in the concerned volume. Because the conductivity σ is projected in computation domain, it will result in numeric dispersion if we use directly discrete approximation for formula (7), Let $E_x(z,t)=\tilde{E}_x(z,t)\,e^{-\sigma' t}$, then

$$\left(\frac{\partial}{\partial z}-\frac{1}{v}\frac{\partial}{\partial t}\right)\tilde{E}_x=0, \tag{8}$$

its finite difference form is

$$E_x^{k+1}(n)=E_x^{k-1}(n)+\frac{2v\Delta t}{\Delta z}\sum_i b(i)\,E_x^k(n+i), \tag{9}$$

The difference form of formula (7) is

$$E_x^{k+1}(n)=e^{-2\sigma'\Delta t}E_x^{k-1}(n)+\frac{2v\Delta t}{\Delta z}e^{-\sigma'\Delta t}\sum_i b(i)\,E_x^k(n+i), \tag{10}$$

where $b(i)=\int\frac{\partial\phi(x)}{\partial x}\phi(x+i-1/2)\,dx$ are the MRTD coefficients.

The UPML material parameters are chosen to be $\sigma_{\xi(\xi=x,y,z)}=0$ for the inner computation region. The maximum value of σ at the end of the UPML region is chosen to be $\sigma_{max}=1/(150\pi\Delta\sqrt{\varepsilon_r})$, where Δ is the cell dimension perpendicular to the UPML interface to the regular region. The UPML region is backed by a perfect electric conductor wall implemented using the mirror principle.

4 Computed results

In microwave circuit analysis, Gauss impulse is generally selected as an excitation for smoothness in time domain and easy spectrum width setting. The width of Gauss pulse is $T=18$ ps, Assume that the time delay $t_0=3T=54$ ps, The response value of the frequency domain can be calculated by Fourier transforming the time domain value.

The circle wave losses of the antenna computed are shown in Fig. 3 and Fig. 4 for $s/a=1$ and $s/a=0.25$, respectively. The computed curves based computation domain $100\times120\times60$ and $\Delta x=\Delta y=0.15$ mm, $\Delta z=0.015$ mm. From Fig. 3 and Fig. 4, we can find the computed results by using FDTD method, and H-MRTD method are in good agreement with measured results. The drifts between them ensured value and the computed value by using FDTD and H-MRTD are about 2% and 2.5% in fine-grid, respectively. The length of the novel patch antenna is less than 1/7 wavelength, the efficiency this novel antenna arrive at 70%. The characteristic parameters such as effective dielectric constant, the characteristic impedance in spectrum domain could be worked out by Fourier transform.

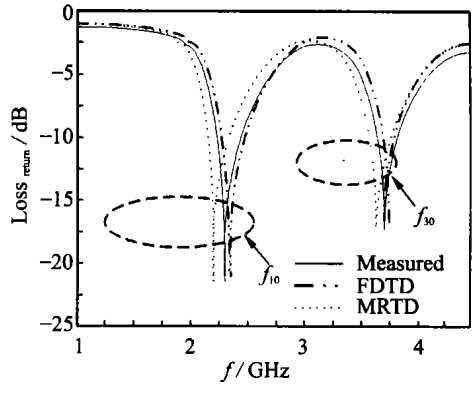

Fig. 3　Computed return loss for $s/a=1$

These simulations were performed by XFDTD, the information about dual-frequency antenna simulations is shown in Tab. 1. We can find when using different space cell sizes, there will be different simulation results. For FDTD method, Although time-step selected satisfied the Courant-Friedrichr-Levy (CFL) condition[13], the accuracy of the simulation results appears diverse when we adopt fine-grid and coarse-grid, re-

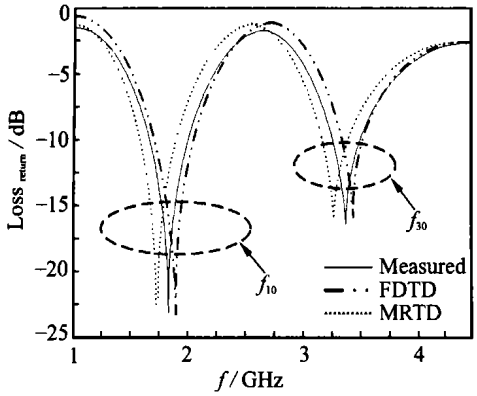

Fig. 4　Computed return loss for $s/a = 0.25$

Tab. 1　Information on the dual-frequency antenna

No. of Yee's cell	Conditions	FDTD	H-MRTD
100× 120× 60	Δt	0.091 5 ns	0.031 5 ns
	Error(%)	±2%	±3.5%
	CPU time(s)	5 300 s	5 340 s
20× 24× 12	Δt	0.138 5 ns	0.089 5 ns
	Error(%)	±12%	±4.5%
	CPU time(s)	3 900	2 000
5× 6× 3	Δt	—	0.1 ns
	Error(%)	—	±5.7%
	CPU time(s)	—	1 000

spectively, it makes clear the numeric errors arrive at 12% in coarse-grid case for FDTD method. It manifests not only time-step but also the size of space-steps affect greatly the numeric errors of FDTD method. If the space-steps change more and more larger, its numeric precision can not be assured. For H-MRTD method, because of the capability of the MRTD algorithms to develop real-time time and space adaptive grids through the efficient thresholding of the wavelet coefficients. Space discretization with only a few cells per wavelength gives accurate results, the influence of the space-steps is smaller than FDTD method, but there are larger numeric errors compared with FDTD method in fine-grid case. Although the time-step of FDTD method is nearly 3 times that of H-MRTD method, The CPU time is quite approximation. This fact is proved to be a serious drawback that the addition of wavelets does not improve significantly the numeric accuracy of the FDTD scheme. It is a hot and highlighted now to study how to improve the numeric accuracy of the H-MRTD method.

5　Conclusion

A dual-frequency miniature patch antenna is presented in this paper, it performs excellently and especially in miniaturization. H-MRTD method was used to model the structure of the antenna. The algorithm of the method is real-time time and space adaptive grids through the efficient thresholding of the wavelet coefficients. Thus, space discretization with only a few cells per wavelength gives accurate results, leading to a reduction of both memory requirement and computation time. The fact that there is a good agreement between the H-MRTD computed values and the measured results or FDTD computed values manifests that the 3-D H-MRTD method is more efficient than the conventional FDTD method. But yet, there still exist some problems, such as the accuracy of numeric simulation and the far field radiation patterns at the two operating frequencies et al, which need to be solved, They will be discussed in our future papers.

参考文献:

[1] Yu W G, Zhong X X, Wu ZH ZH, *et. al*. Novel stack-shorted microstrip bluetooth antenna[J]. *Optics and Precision Engineering*, 2003, 11(4): 394-399.

[2] LIU ZH F, KOOI P SH, *et. al*. A method for designing broad-band microstrip antenna in multilayered planar structures[J]. *IEEE Trans Antennas and Propagat*, 1999, 47(9): 1416-1420.

[3] YU W G, ZHONG X X, WU ZH ZH, *et al*. Numerical analysis of micromachine patch antenna using FDTD technique[C]. *The International Computer Science Conference* 2003. *Active Media Technology (ICAMT* 2003). Chongqing, China. 2003, 29-31, 346-351.

[4] WU ZH ZH, ZHONG X X, LI X Y, *et al*. Multiplayer-shorted micromachined Bluetooth antenna[J]. *Optics and Precision Engineering*. 2001, 9(6): 572-576.

[5] ZAID L, KOSSIAVAS G, *et al*. Dual-frequency and broad-band antennas with stacked quarter wavelength elements[J]. *IEEE Trans*, 1999, AP-47(4): 654-660.

[6] YEE K S. Numerical solution of initial boundary value problems involving Maxwell's equation in isotropic media[J]. *IEEE Trans Antennas Propagation*, 1966, 14(5): 302-307.

[7] KRUMPHOLZ M, KATEHI L P B. MRTD: new time-domains schemes based on multiresolution analysis[J]. *IEEE Trans Microwave Theory Tech*, 1996, 44(4): 555-571.

[8] TENTZERIS E, ROBERTSON R, CANGELLARIS A, *et al*. Space- and time-adaptive gridding using MRTD[C]. *Proc. MTT-S*, 1997. 337-340.

[9] TENTZERIS E, HARVEY J, KATEHI L P B. Time adaptive time-domain techniques for the design of microwave circuits[J]. *IEEE Microwave and Guided Wave Letters*, 1999, 9(3): 96-98.

[10] GEDNEY S D. An anisotropic perfectly matched layer absorbing media for the truncation of FDTD lattices[J]. *IEEE Trans Antennas and Propagation*, 1996, 44(12): 1630-1639.

[11] MAC S, BIFFI G G, PIAZZESL P, *et al*. Dual-band slot-loaded patch antenna[C]. *IEE Proc Microw Antennas Propag*, 1995, 142(3): 225-232.

[12] CHEONG Y W, LEE Y M, RA K H, *et al*. Wavelet-Galerkin scheme of time-dependent inhomogeneous electromagnetic problems[J]. *IEEE Microwave Guided Wave Lett*, 1999, 9(8): 297-299.

[13] TAFLOVE A, BRODWIN M E, Numerical solution of steady state electromagnetic scattering problem using the time dependent Maxwell's equations [J]. *IEEE Trans MTT*, 1975, 23(8): 623-630.

作者简介: 余文革(1967-), 男, 四川渠县人, 重庆大学光电工程学院博士研究生, 主要研究方向为 MEMS 天线及电磁场数值分析;

钟先信(1935-), 男, 重庆人, 重庆大学光电工程学院教授, 博士生导师, 主要研究方向为精密机械及 MEMS。